

Weighting Factor Design in Model Predictive Control of Power Electronic Converters: An Artificial Neural Network Approach

Tomislav Dragičević , Senior Member, IEEE, and Mateja Novak , Student Member, IEEE

Abstract—This paper proposes the use of an artificial neural network (ANN) for solving one of the ongoing research challenges in finite set-model predictive control (FS-MPC) of power electronics converters, i.e., the automated selection of weighting factors in cost function. The first step in this approach is to simulate a detailed converter circuit model or run experiments numerous times using different weighting factor combinations. The key performance metrics [e.g., average switching frequency (f_{sw}) of the converter, total harmonic distortion, etc.] are extracted from each simulation. This data is then used to train the ANN, which serves as a surrogate model of the converter that can provide fast and accurate estimates of the performance metrics for any weighting factor combination. Consequently, any arbitrary user-defined fitness function that combines the output metrics can be defined and the weighting factor combinations that optimize the given function can be explicitly found. The proposed methodology was verified on a practical weighting factor design problem in FS-MPC regulated voltage source converter for uninterruptible power supply system. Designed weighting factors for two exemplary fitness functions turned out to be robust to load variations and to yield close to expected performance when applied both to detailed simulation model (less than 3% error) and to experimental test bed (less than 10% error).

Index Terms—Artificial neural network (ANN), finite set-model predictive control (FS-MPC), voltage source converter (VSC), weighing factor design.

I. INTRODUCTION

POWER electronic converters are a key enabling technology for the integration of renewable energy sources, HVdc transmission systems, and electric vehicle charging infrastructure in the electric power system [1]. They are also basic building blocks of variable speed electrical drives, as well as architectures, such as microgrids and uninterruptible power supply (UPS) systems [2]. Among different converter topologies, voltage source converters (VSC) are the most

Manuscript received May 18, 2018; revised September 9, 2018; accepted October 1, 2018. Date of publication October 17, 2018; date of current version June 28, 2019. (Corresponding author: Tomislav Dragičević.)

The authors are with the Department of Energy Technology, Aalborg University, 9220 Aalborg East, Denmark (e-mail: tdr@et.aau.dk; nov@et.aau.dk).

Color versions of one or more of the figures in this paper are available online at <http://ieeexplore.ieee.org>.

Digital Object Identifier 10.1109/TIE.2018.2875660

widely spread in practice. Large number of advanced control techniques for VSCs have been proposed over the past years, aiming to mitigate some of the well-known limitations of classical linear control approaches [3].

These often cited limitations comprise slow transient performance, low robustness to parameter variations, and lack of flexibility to effectively balance multiple control objectives. Among different alternative approaches that could potentially offer better control characteristics in these aspects, model predictive control (MPC) can be singled out as one of the most promising ones. Particularly, the finite set MPC (FS-MPC) takes advantage of the discrete model of the converter to predict its future behavior for every possible switching configuration. The predicted numerical values of converter's state variables at the next sampling step are then used in the cost function that defines the desired performance of the system [4]. This approach yields a simple and intuitive implementation, where constraints of the state variables can be explicitly dealt with. In addition, a number of performance objectives can be balanced by properly selecting the weighting factors associated with each objective. Due to these benefits, FS-MPC has been applied to numerous power electronic applications in the recent years [5]–[10].

Despite the significant research progress, there are still several open research issues with the FS-MPC [11]. First one is that FS-MPC algorithms typically yield a variable switching frequency at the output of converter, which is often undesirable. Namely, the wide harmonic spectrum not only increases the risk of triggering unexpected resonances, but it also complicates the converter filter design. Several approaches have been reported to tackle the variable switching frequency issue. Some examples are filtering the cost function [12], introducing upper and lower bounds on the number of switching instances [13], and implementing modulated [14] or quasi-modulated MPC algorithms [15].

Another issue is that the selection of suitable weighting factors in the cost function to achieve optimal balance between the objectives is not trivial. In fact, the most commonly used methodology is carrying out time-consuming simulations and relying on trial-and-error approach to test the effect of different weighting parameter combinations [16]. As one of the first propositions to reduce the time effort to some extent, branch and bound search variant has been proposed in [17]. Nevertheless, the weighting factor selection in that work is still empirical.

A fully automated approach was proposed in [18], where an iterative simulation procedure aided by genetic algorithm optimization was deployed to draw some conclusions about suitable design of the two weighting factors in the cost function. However, although automated, this method is heuristic and very time consuming as it requires to run a new set of simulations for every design objective. Moreover, the methodology was not experimentally verified. On the other hand, an online weighting factor adaptation scheme was proposed in [19]. Here, the analytical torque ripple expression was used as a basis to explicitly derive the optimal weighting factor as a function of design parameters and measured variables. However, the proposed method was only used to minimize the torque ripple, while switching frequency was left uncontrolled. In addition, online evaluation of complex functions can significantly increase the computational burden, which could make it impractical for implementation on cheap commercial microprocessors.

In sharp contrast to these techniques, weighting factors were completely avoided in [20] and [21]. In [20], this is done by transforming the cost function based MPC formulation into a multiobjective optimization problem. Nevertheless, the membership functions that represent individual terms in the cost function still require priority coefficients that can only be heuristically chosen. On the other hand, an inverse model of the plant is used in [21] to explicitly calculate the actuation that will drive the torque and flux error to zero. However, this approach is only suitable for systems where it is possible to have multiple controlled variables simultaneously at zero error. Therefore, this method is not applicable for cost functions with multiple conflicting control objectives. To sum up, the existing approaches without weighting factors are not flexible enough for straightforward application to any generic power electronic system. On the other hand, none of the approaches for designing cost functions with weighting factors allow their explicit selection that guarantees the optimal performance of the system according to some user-defined design criteria.

This paper proposes a possible solution to this long-standing research problem with the use of an artificial neural network (ANN) for automated selection of the weighting factors in the MPC cost function. The first step in this approach is to test the behavior of converter numerous times, each time with a different weighting factor combination. This can be done either using a detailed simulation model or experimentally. The metrics that quantify the performance of the converter [e.g., total harmonic distortion (THD), average switching frequency f_{sw} , or/and others as needed] are then extracted from each test. Obtained data is then organized into input/output matrix where elements in every row correspond to the combination of weighting factor values and associated performance metrics from one simulation. This data is used to train the ANN, which can serve as a fast surrogate model of the power converter, thus allowing fast and automatic selection of the optimal weighting factors.

The paper is organized as follows. Principle of the FS-MPC and the UPS converter case study, which is investigated in detail in this paper, are introduced in Section II. Section III proposes the ANN-based weighting factor design methodology. It also provides the fundamentals of ANNs, describing both their

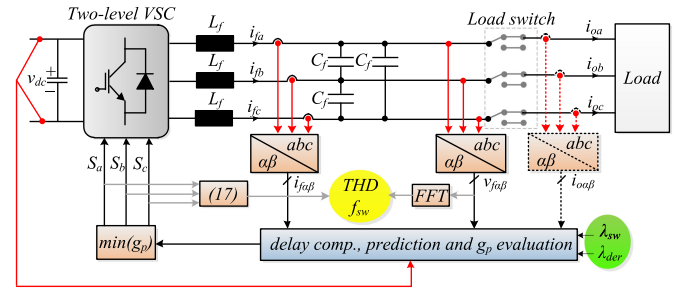


Fig. 1. Structure of the FS-MPC regulated VSC for UPS applications. Weighting factors λ_{der} and λ_{sw} (highlighted with green color) affect the performance metrics of the system like voltage THD and average switching frequency f_{sw} (highlighted with yellow color).

structure and the training procedures. Section IV then focuses on applying the proposed method on the FS-MPC regulated UPS converter example, detailing all the steps starting from the data generation process, training the ANN, and finally finding the optimal weighting factors according to the two different design criteria. Experimental results are provided in Section V, while conclusions and some suggestions for the future work are given in Section VI.

II. FS-MPC PRINCIPLE

Fig. 1 shows the FS-MPC regulated VSC suitable for the UPS application. FS-MPC uses the model of the converter to predict its behavior in the future for all possible switching configurations, starting from the most recent measurements. These predictions are then evaluated with a cost function that defines the desired performance of the system. Finally, the switch configuration that is associated with the least value in the cost function is the optimal one and it is applied to the converter. Next section describes the model of the converter.

A. Converter Model

Standard two-level VSC is considered in this paper. It can be modeled in a stationary $\alpha\beta$ reference frame. For this reason, all three-phase variables x_a , x_b , and x_c , are transformed into a corresponding $\alpha\beta$ frame by applying an amplitude-invariant Clarke transformation T

$$\bar{x} = x_\alpha + jx_\beta = T[x_a \ x_b \ x_c]' \quad (1)$$

where

$$T = \frac{1}{3} \begin{bmatrix} 2 & -1 & -1 \\ 0 & \sqrt{3} & -\sqrt{3} \\ 1 & 1 & 1 \end{bmatrix}. \quad (2)$$

The three gating signals S_a , S_b , and S_c determine the voltages of legs a , b , and c . Each leg can be in two states, and thus the VSC can be in $2^3 = 8$ configuration in total. The potential of the middle point of any inverter leg with respect to the point N can be obtained by multiplying v_{dc} with the associated gating signal, as $v_{aN} = S_a \cdot v_{dc}$, $v_{bN} = S_b \cdot v_{dc}$, and $v_{cN} = S_c \cdot v_{dc}$. It is noted that the dc-link voltage is assumed ideal since it is tightly regulated by a separate front-end converter. There also

TABLE I
COMPLEX VOLTAGE VECTORS USED IN TWO-LEVEL THREE-PHASE VSC

S_a	S_b	S_c	Voltage vector \bar{v}_i
0	0	0	$\bar{v}_0 = 0$
1	0	0	$\bar{v}_1 = \frac{2}{3}v_{dc}$
1	1	0	$\bar{v}_2 = \frac{1}{3}v_{dc} + j\frac{\sqrt{3}}{3}v_{dc}$
0	1	0	$\bar{v}_3 = -\frac{1}{3}v_{dc} + j\frac{\sqrt{3}}{3}v_{dc}$
0	1	1	$\bar{v}_4 = -\frac{2}{3}v_{dc}$
0	0	1	$\bar{v}_5 = -\frac{1}{3}v_{dc} - j\frac{\sqrt{3}}{3}v_{dc}$
1	0	1	$\bar{v}_6 = \frac{1}{3}v_{dc} - j\frac{\sqrt{3}}{3}v_{dc}$
1	1	1	$\bar{v}_7 = 0$

exists a common mode voltage drop v_{nN} that results in reduced voltage across the filter

$$v_{nN} = \frac{v_{aN} + v_{bN} + v_{cN}}{3}. \quad (3)$$

The voltages across the filter can then be expressed as $v_{an} = v_{aN} - v_{nN}$, $v_{bn} = v_{bN} - v_{nN}$, and $v_{cn} = v_{cN} - v_{nN}$. Finally, the Clarke transformation, given in (1) and (2), is applied to the filter voltages for all possible gating signal combinations, to obtain their expressions in the stationary $\alpha\beta$ frame.

All possible voltage vectors, represented as \bar{v}_i , are shown in Table I. They are applied to the LC filter, which can be described by differential equations of the inductor current \bar{i}_f and capacitor voltage \bar{v}_f , as follows:

$$\begin{aligned} L_f \frac{d\bar{i}_f}{dt} &= \bar{v}_i - \bar{v}_f - R_f \bar{i}_f \\ C_f \frac{d\bar{v}_f}{dt} &= \bar{i}_f - \bar{i}_o \end{aligned} \quad (4)$$

where \bar{i}_o is the output current.

For convenience, (4) can be expressed in the state-space form as

$$\frac{d}{dt} \begin{bmatrix} \bar{i}_f \\ \bar{v}_f \end{bmatrix} = \mathbf{A} \begin{bmatrix} \bar{i}_f \\ \bar{v}_f \end{bmatrix} + \mathbf{B} \begin{bmatrix} \bar{v}_i \\ \bar{i}_o \end{bmatrix} \quad (5)$$

where

$$\mathbf{A} = \begin{bmatrix} -R_f & -\frac{1}{L_f} \\ \frac{1}{C_f} & 0 \end{bmatrix} \quad (6)$$

and

$$\mathbf{B} = \begin{bmatrix} \frac{1}{L_f} & 0 \\ 0 & -\frac{1}{C_f} \end{bmatrix}. \quad (7)$$

The equations above define the continuous state-space model of a two-level three-phase VSC. To obtain discrete representation suitable for digital control implementation, the zero-order hold discretization method is used to ensure that the discrete-time model coincides with the continuous model at the sampling

instants

$$\begin{bmatrix} \bar{i}_f(k+1) \\ \bar{v}_f(k+1) \end{bmatrix} = \mathbf{A}_d \begin{bmatrix} \bar{i}_f(k) \\ \bar{v}_f(k) \end{bmatrix} + \mathbf{B}_d \begin{bmatrix} \bar{v}_i(k) \\ \bar{i}_o(k) \end{bmatrix}. \quad (8)$$

B. Cost Function

After the model is set up, the suitable cost function needs to be defined to evaluate which actuation should be applied at the next sampling instant. Cost functions with the prediction horizons of various lengths have been proposed in power electronics applications to improve the steady-state performance of the converter [7], [22]. As discussed in [7], multistep prediction horizons are useful at lower switching frequencies, which are common to high-power multilevel converters. On the other hand, for simple converter topologies operated with higher switching frequencies, a single-step prediction is usually the more suitable choice. Namely, only limited performance gain can be obtained by using longer prediction horizons [23]. Moreover, single-step horizon is simpler to implement with less computational burden, and allows excellent flexibility to integrate linear and nonlinear control objectives and constraints. Cost function with single-step prediction horizon is used for the case study paper, as described next. However, it is important to highlight that the weighting factor design method proposed in the following section is generic and thus suitable to deal with any length of prediction horizon and any type of converter topology.

For ac voltage regulation on the LC filter of the UPC converter, the single-step horizon cost function can be expressed as follows [5]:

$$g_{\text{con}} = (v_{f\alpha}^* - v_{f\alpha})^2 + (v_{f\beta}^* - v_{f\beta})^2 \quad (9)$$

where $\bar{v}_f^* = V_r e^{j\omega_r} = v_{f\alpha}^* + jv_{f\beta}^*$ is the voltage reference, with V_r and $\omega_r = 2\pi f_r$ being its amplitude and the angular frequency, respectively.

Additional current reference term, which is actually a derivative of the load reference voltage, was proposed in [10] to improve the steady-state performance

$$g_c = (C_f \omega_r v_{f\beta}^* - i_{f\alpha} + i_{o\alpha})^2 + (C_f \omega_r v_{f\alpha}^* + i_{f\beta} - i_{o\beta})^2. \quad (10)$$

The g_c term is multiplied with a weighting factor λ_{der} and added to (9). Moreover, the current limiting term h_{lim} , and switching penalization term sw , are also introduced

$$h_{\text{lim}} = \begin{cases} 0, & \text{if } |\bar{i}_f| \leq i_{\max} \\ \infty, & \text{if } |\bar{i}_f| > i_{\max} \end{cases} \quad (11)$$

$$sw = |\Delta S_a(i)| + |\Delta S_b(i)| + |\Delta S_c(i)| \quad (12)$$

where $|\Delta S_a(i)|$ is 1 if switch change occurs in leg a at instant i and 0 otherwise. The same is valid for leg b and leg c .

Finally, all these terms are integrated into a complete cost function

$$g_p = g_{\text{con}} + \lambda_{\text{der}} g_c + h_{\text{lim}} + \lambda_{\text{sw}} sw^2. \quad (13)$$

As it can be seen, two weighting factors should be selected, i.e., λ_{der} and λ_{sw} . The selection of these parameters has a strong influence on the performance of the system. Important metrics

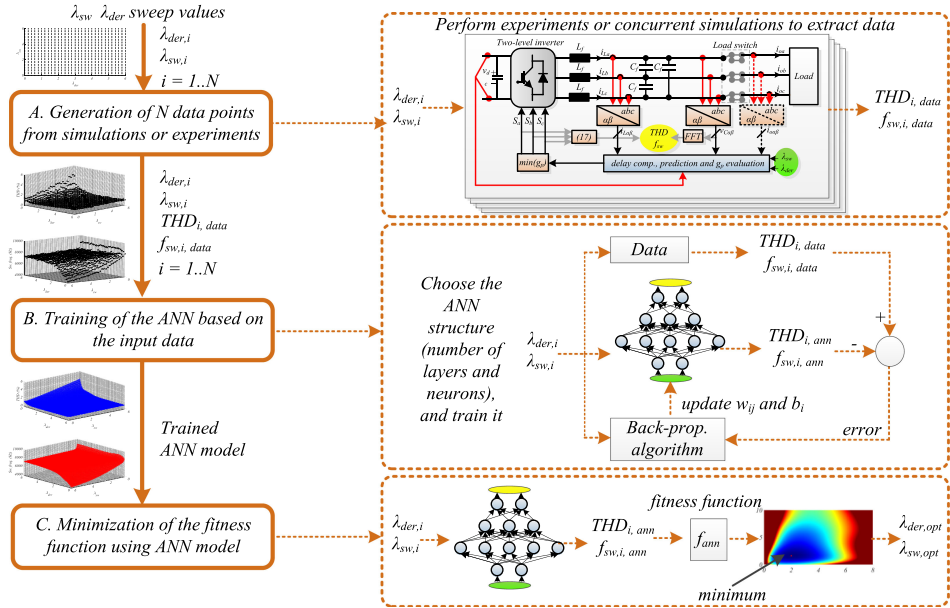


Fig. 2. Flow diagram of the proposed ANN-based design of the weighting factors in the model predictive control of power electronic converters.

that quantify this performance are the THD of the capacitor voltage and average switching frequency f_{sw} of the converter. The design parameters and performance metrics are highlighted in Fig. 1 with green and yellow color, respectively. In this paper, we propose an ANN-based approach to design these weighting factors in a fully automated and fast way. It should be mentioned that only steady-state performance metrics are considered here because the selection of the weighting factors in this case study have a negligible influence on the dynamic performance metrics of the system. This will also be demonstrated in later sections. On the other hand, there are applications in which it is worth to consider the influence of weighting factors on dynamic performance. For instance, it has been shown in [24] that one of the weighting factors has an influence on the phase margin of the system. In this case, the phase margin should be considered as additional performance metric, but the principle in the proposed method would remain the same.

III. PROPOSED ANN-BASED WEIGHTING FACTOR DESIGN APPROACH

In this section, the proposed weighting factor design methodology is introduced first. Since the ANN plays an instrumental role in it, the details about its structure and training procedures are summarized as well.

A. Proposed Methodology

Overall workflow of the proposed approach is shown in Fig. 2. Three main steps, i.e., A, B, and C can be identified from the figure. The goal of step A is to extract the voltage THD and average f_{sw} for every combination (out of N possible combinations) of input parameters λ_{der} and λ_{sw} . The THD and average f_{sw} could be extracted either from a detailed simulation model or experimentally. In any case, the weighting factor sweep should

be organized in such a way to cover a feasible design space with some reasonable fidelity.

If data is extracted from the simulation model, the process can be accelerated with parallel computing. On the other hand, if data is extracted experimentally, it could be done either in automated fashion or manually. Automated procedure can easily be programmed on a standard microprocessor. For instance, the weighting factors can be adjusted in real time on the platform, while voltage waveforms and average f_{sw} can be automatically recorded and stored for later analysis. It should be noted that experimental data extraction might be the only option if one has to deal with a commercial power electronic product, as detailed simulation models are generally not available for such products. However, there are several risks associated with this approach. For instance, the product may be damaged if unfeasible combination of weighting factors is tested. Therefore, the data extraction from experimental test bed should always be carefully monitored by a human operator. For this reason, experimental data extraction may be extremely lengthy procedure considering that hundreds or even thousands of experiments need to be carried out and that the workload cannot be parallelized as it is the case with the simulations. Therefore, the case study in this paper is carried out using the data extraction from the simulation model. A detailed discussion about the acceleration of the total simulation workload with parallel computing is also provided in Section IV-D.

In step B, we take the advantage of data obtained in step A to train the ANN, which then becomes a fast surrogate model of the converter. The trained ANN can provide accurate voltage THD and average f_{sw} estimations for any given λ_{der} and λ_{sw} combination, several orders of magnitudes quicker than the detailed simulation. It is worth noticing that steps A and B need to be performed only once for a given converter topology and operating conditions. Once the ANN is trained, it can be used in

step *C* as a basis for evaluating some user-defined fitness function f_{ann} that can combine the desired voltage THD and average f_{sw} in any arbitrary way, where λ_{der} and λ_{sw} combinations that minimize f_{ann} can be found almost instantaneously.

B. ANN Structure and Training

Numerous types of ANNs have been proposed in the literature by now [25]. Proper selection of the particular network depends mostly on the nature of relationships between inputs and outputs in the data. For sequential data, where future outputs depend on past values of the inputs and outputs, recurrent neural networks are a good choice. On the other hand, since the relationship between weighting factors and performance metrics can be considered static, forward ANN has been selected for the case study in this paper. Forward ANNs are the commonly used machine learning algorithms for various electrical engineering problems, from predicting the voltage distortion in electrical distribution networks [26], to designing the microwave filters [27], [28].

A feed-forward ANN consists of an input layer, one or more hidden layers, and an output layer. Each layer comprises a number of neurons that process the information coming from neurons in the layer below. To calculate the output of a certain neuron γ_i^l in layer l , the outputs of all the neurons z_j^{l-1} ($j = [1 \dots N_{l-1}]$) in the layer immediately below $l - 1$ are multiplied with associated weights w_{ij}^l and summed up together with the bias term b_i^l . The result is processed through an activation function σ that usually takes the form of a sigmoid function, i.e., $\sigma(\gamma) = 1/(1 + e^{-\gamma})$, to generate output z_i^l . This output then becomes one of the inputs for the layer above, $l + 1$. The same procedure is done to calculate the output of other neurons in layer l .

In the input layer, z_i^1 simply takes the form of inputs. On the other hand, the output layer typically uses the linear activation function to allow any numerical value, as opposed to being limited to $[0, 1]$ range with sigmoid function. The complete signal flow of the ANN can be described as follows.

1) Layer 1 (input):

$$z_i^1 = x_i \quad i = 1, \dots, N_1 \quad (14)$$

where x_i are the inputs.

2) Layers $l = 2, \dots, L - 1$ (hidden)

$$z_i^l = \sigma \left(\sum_{j=1}^{N_{l-1}} w_{ij}^l z_j^{l-1} + b_i^l \right) \quad i = 1, \dots, N_l. \quad (15)$$

3) Layer L (output):

$$y_i = w_i^L z_i^L \quad i = 1, \dots, N_L \quad (16)$$

where y_i are the outputs.

An example of one ANN is shown in Fig. 3. It can be seen that this network has an input layer, two hidden layers, and an output layer. Therefore, there are four layers ($L = 4$) in total. The number of neurons in the input layer are two ($N_1 = 2$) since there are two design parameters λ_{der} and λ_{sw} (marked with green color, as in Fig. 1). This means that $x_1 = \lambda_{\text{der}}$ and $x_2 = \lambda_{\text{sw}}$. The number of layers in the two hidden layers are 5 and 3, respectively ($N_2 = 5, N_3 = 3$). As elaborated in the following section, it was empirically determined that such ANN

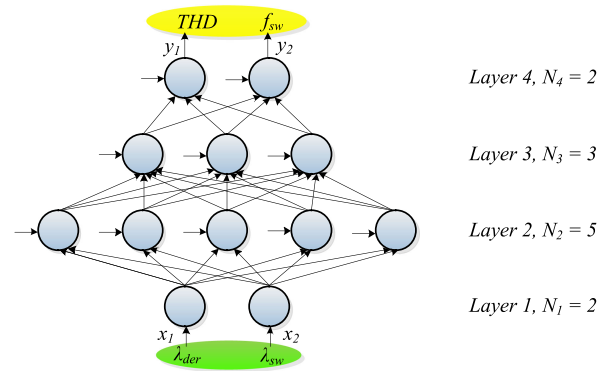


Fig. 3. ANN that serves as a surrogate model of the original UPS converter shown in Fig. 1. For simplicity weights and bias terms are omitted from the figure. As in Fig. 1, the inputs to the ANN are highlighted with green color, while the outputs with yellow.

structure yields the best response for the case study presented in this paper. The output layer comprises two neurons ($N_4 = 2$) because our design interest is in two performance indicators, i.e., the converter average switching frequency f_{sw} and THD (marked with yellow color, again as in Fig. 1 to highlight the link between the detailed converter model and its ANN surrogate). Thus, $y_1 = \text{THD}$ and $y_2 = f_{\text{sw}}$.

It has been shown in [29] that forward ANN is an universal function approximator, i.e., that the weights and bias terms in its structure can be adjusted in such a way to approximate any given input/output data relationship with arbitrary precision, given that the number of neurons is sufficient. The process of adjusting these parameters is typically done using the back-propagation algorithm. This algorithm takes advantage of the continuous differentiability of the ANN to find out the direction in which the w_{ij}^l and b_i^l parameters should be adjusted in each training iteration to reduce the error between the measured output data and prediction made by the ANN from previous iterations (see the middle right part in Fig. 2) [30]. Back propagation is a very well-known algorithm that is available in standard software like MATLAB. Therefore, it will not be described further here. Next section applies the proposed method on the practical case study of the UPS converter.

IV. WEIGHTING FACTOR DESIGN FOR THE UPS CONVERTER

In this section, we verify the proposed design methodology on an FS-MPC regulated UPS converter case study that was described in detail in Section II. Steps *A* and *B* from Fig. 2 are presented next, while step *C* is demonstrated for the two design examples in Section IV-C.

A. Data Generation Procedure

In order to generate the data, a detailed simulation model of the FS-MPC regulated VSC used for UPS application was developed in MATLAB/Simulink. The structure of simulation model corresponds to a block diagram presented in Fig. 1, where the parameters used are given in Table II. Data has been extracted for two different load values ($R_{\text{load}} = 60 \Omega$ and $R_{\text{load}} = 120 \Omega$) in order to check the robustness of weighting factor designs to changing load conditions. In order to enforce as close

TABLE II
PARAMETERS OF THE TEST SYSTEM USED IN SIMULATIONS
AND EXPERIMENTS

DC link voltage	$v_{dc} = 700 \text{ V}$
Sampling time for control	$T_s = 20 \mu\text{sec}$
Converter dead time	$T_d = 4 \mu\text{s}$
Time step (in simulation)	$T_{sim} = 1 \mu\text{sec}$
<i>LC</i> -filter	$L_f = 2.4 \text{ mH}, C_f = 15 \mu\text{F}$
Reference voltage	$V_r = 326.6 \text{ V}, f_r = 50 \text{ Hz}$
Nominal load	$R_{load} = 60 \Omega$
Light load	$R_{load} = 120 \Omega$

resemblance as possible between the simulation model and experimental system, a computational delay of one sampling time T_s and dead times T_d have been modeled as well.

A range of λ_{der} and λ_{sw} sweep was chosen from 0 to 10, with a step of 0.5 to cover the practical design range with high fidelity. Particularly, 21 settings for each parameter were tested, which means that there were $N = 21^2 = 441$ weighting parameter combinations to be simulated for each load value. Each simulation was set to last for 0.06 s (three fundamental cycles), where THD and average switching frequency were automatically calculated at the end of each simulation. Fast Fourier transform algorithm available in the MATLAB/SimPowerSystems toolbox was used for the THD calculations, while the average f_{sw} was calculated with following equation, as also indicated in Fig. 1:

$$f_{sw} = \sum_{i=1}^{3000} \frac{|\Delta S_a(i)| + |\Delta S_b(i)| + |\Delta S_c(i)|}{6}. \quad (17)$$

The summation was done until 3000 because in the 0.06-s period, this was the number of sampling instants considering the $20 \mu\text{s}$ duration of the sampling step. The automated simulation setup was programmed using the Matlab/Parallel Computing toolbox. Simulations were then carried out on a standard personal computer with four cores, and all the results were obtained within around 22 min (11 min for each load value). The input/output data was also normalized. To this end, the largest value of a each variable was used as its norm and all other values of the same variable were then divided by the norm prior to the training. Next, as described in the step *B* of Fig. 2, the suitable structure of the ANN was determined and two normalized datasets were used to train two ANNs (each for a different load value).

B. ANN Model Development

After the data has been generated and before proceeding with the ANN training, it is first necessary to determine the suitable ANN structure. This step can generally be carried out empirically, by trying ANN structures with one or more hidden layers and different numbers of neurons in each layer. These tryouts can be done relatively fast since the training of one ANNs takes only around 1 s. The number of hidden layers was chosen to be two in this case study, as it turned out that less neurons in total are needed to achieve excellent matching with the training data compared to the case when only one hidden layer is used.

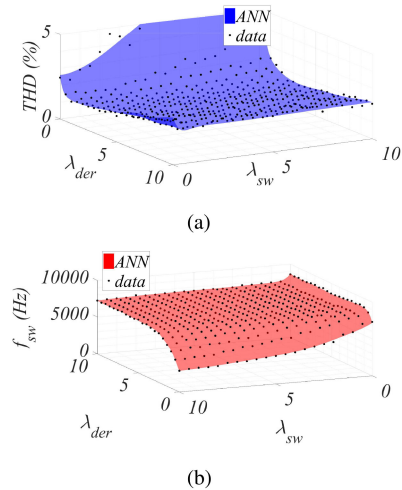


Fig. 4. Comparison between the data generated through simulation model corresponding to Fig. 1 and trained ANN shown in Fig. 3. (a) Comparison between the THD obtained from detailed simulation model and from the ANN for the light load. (b) Comparison between the f_{sw} obtained from detailed simulation model and from the ANN for the light load.

Nevertheless, structure with one hidden layer could also be used to produce the response of virtually the same quality.

After selecting the number of layers, next step was to determine the best number of neurons in each layer. The main issues that arose from nonsuitable selection of the number of neurons were underfitting and overfitting. For instance, if there were too few neurons (e.g., 2 and 1 in first and second hidden layer, respectively), the network was overly simplistic, and it was not able to capture well the training data (underfitting). On the other hand, when the number of neurons was too large (e.g., 100 and 20, respectively), the trained network achieved good match with the training examples, but failed to find the natural structure of the input/output data relationships (overfitting). Eventually, the ANN structure with 5 and 3 in first and second hidden layer (see Fig. 3) turned out to be the simplest network that provides excellent response. It was also noticed that many other combinations with higher number of neurons provided a negligible difference in response, thus indicating the robustness of the ANN design. The comparison between the predicted outputs by the best-fit ANNs and original data for light load example using the ANN structure shown in Fig. 3 can be seen in Fig. 4(a) and (b). The figures indicate good matching with detailed simulation data. Since very similar figures were also observed for the nominal load case, the latter are not shown here.

C. Design Examples

Final step was to use the two trained ANNs to find the optimal λ_{der} and λ_{sw} settings for achieving two exemplary performance goals of the system. To visualize the impact of these factors, high fidelity plots of the fitness functions have been drawn using data generated through trained ANNs. In particular, approximately 4 million fitness function points have been evaluated through each trained ANN in less than 0.5 s. As a comparison, it takes around 6 s to simulate a detailed VSC circuit for only one set of design parameters. Such a speed permitted the use of an

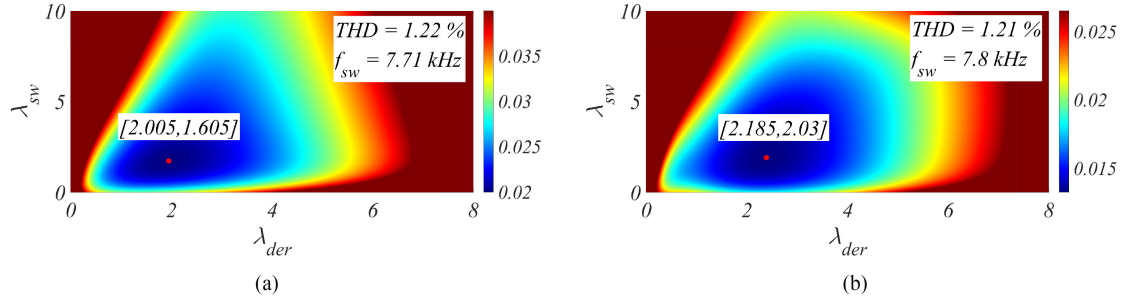


Fig. 5. Optimal weighting factors for the fitness function (18). (a) Plot of the fitness function (18) for the nominal load. Optimal weighting factors (indicated by the red dot) are found to be $\lambda_{der} = 2.005$, and $\lambda_{sw} = 1.605$, resulting in predicted THD of 1.22 % and $f_{sw} = 7.71$ kHz. Simulation of detailed model using the same weighting factors resulted in measured THD = 1.22% and $f_{sw} = 7.64$ kHz. (b) Plot of the fitness function (18) for the light load. Optimal weighting factors (indicated by the red dot) are found to be $\lambda_{der} = 2.185$, and $\lambda_{sw} = 2.03$, resulting in predicted THD of 1.21% and $f_{sw} = 7.8$ kHz. Simulation of detailed model using the same weighting factors resulted in measured THD = 1.28% and $f_{sw} = 7.7$ kHz.

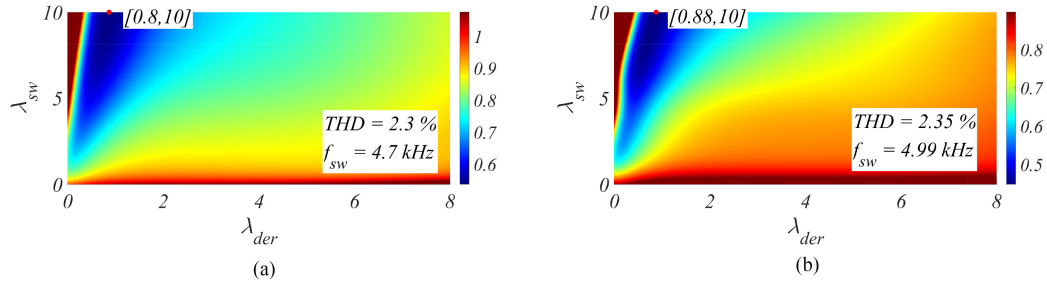


Fig. 6. Optimal weighting factors for the fitness function (19). (a) Plot of the fitness function (19) for the nominal load. Optimal weighting factors (indicated by the red dot) are found to be $\lambda_{der} = 0.8$, and $\lambda_{sw} = 10$, resulting in predicted THD of 2.3% and $f_{sw} = 4.7$ kHz. Simulation of detailed model using the same weighting factors resulted in measured THD = 2.32% and $f_{sw} = 4.7$ kHz. (b) Plot of the fitness function (19) for the light load. Optimal weighting factors (indicated by the red dot) are found to be $\lambda_{der} = 0.88$, and $\lambda_{sw} = 10$, resulting in predicted THD of 2.35% and $f_{sw} = 4.99$ kHz. Simulation of detailed model using the same weighting factors resulted in measured THD = 2.58% and $f_{sw} = 4.55$ kHz.

exhaustive search algorithm for finding the minimum of the fitness function that corresponds to the optimal set of weighting factors. On the other hand, for more complex problems, the computational burden may become too high for exhaustive search. This issue and possible remedies are discussed in detail in Section IV-D. The two particular design examples are presented below.

1) Minimization of the THD: The first objective was defined to find the settings that provide the minimum possible THD

$$f_{\text{ann},1} = \text{THD}_{\text{ann}}^2. \quad (18)$$

The two plots of this fitness function derived through the ANN model, where each one corresponds to a different load value, are shown in Fig. 5(a) and (b), respectively. Surprisingly, the best λ_{sw} in both cases turned out not to be 0, but approximately 1.6 and 2. The best λ_{der} were found to be 2.005 and 2.185. However, it is worth noticing that the precise selection of parameters is not of large importance, especially for λ_{der} that allows quite wide range of values to still yield performance that is very close to optimal. It can thus be concluded that the same weighting factors could safely be chosen for both load cases, which indicates robustness of the selection strategy to load variations. The predicted THDs and f_{sw} were also very similar for both load cases.

In order to illustrate the validity of these results, the detailed VSC simulation was carried out. Only the capacitor voltage waveforms for nominal load have been presented due to limited

space [see Fig. 7(a)]. The calculated THDs were 1.22% and 1.28%, while f_{sw} were 7.64 and 7.7 kHz, respectively. The prediction error of ANN was thus less than 3% in both cases.

2) Minimization of the THD With Low f_{sw} : Second objective was defined to find the settings that provide the best possible THD, but favoring low average switching frequency. This was formulated as follows:

$$f_{\text{ann},2} = 3 \cdot \text{THD}_{\text{ann}}^2 + (\text{freq}_{\text{ann}})^2. \quad (19)$$

Factor 3 was chosen to give more importance to THD minimization, thus keeping it still relatively low. Nevertheless, selecting any other coefficient different than 3 in (19) would provide us with the combination of weighting factors that still guarantees the optimal tradeoff between THD and switching frequency, but they would have different values. This simply means that for a given switching frequency, it is not possible to get a lower THD. Similarly, for a given THD, it is not possible to get a lower switching frequency. Indeed, by making a sweep of coefficient in (19), one would obtain the two-dimensional Pareto front that reveals the tradeoff between the THD and switching frequency (and also the associated weighting factors for each point on the Pareto front).

The plot showing values of fitness function (19) is shown in Fig. 6(a) and (b). In this case, optimal λ_{sw} turned out to be 10 in both cases, while best λ_{der} was found to be 0.8 and 0.85. Of course, even higher settings of λ_{sw} could be used, but the predicted THD and f_{sw} would not be so accurate since the

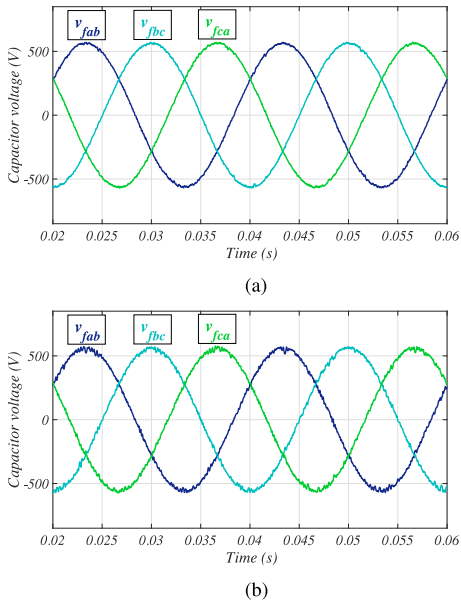


Fig. 7. Capacitor voltage waveforms obtained from detailed simulation model with nominal load for weighting factors that optimize fitness functions (18) and (19), respectively. (a) Waveforms for nominal load with $\lambda_{der} = 1.605$ and $\lambda_{sw} = 2.005$. (b) Waveforms for nominal load with $\lambda_{der} = 0.8$ and $\lambda_{sw} = 10$.

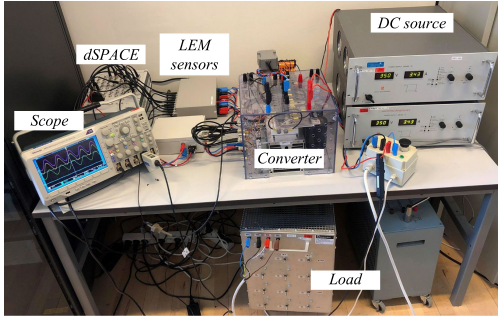


Fig. 8. Caption of the experimental test bed for the UPS converter.

weighting factor settings would be out of the ANN training range. In addition, increasing the weighting factor λ_{sw} beyond the value of 10 would further reduce the switching frequency and increase the THD, even above permissible limits defined by relevant standards (e.g., IEC 62040-3). Therefore, using a larger weighting factor range than 0–10 does not have much practical relevance and would thus unnecessarily increase the overall computational burden (see Section IV-D for detailed discussion). The predicted THDs in this case were 2.3% and 2.35%, while f_{sw} were 4.7 and 4.99 kHz, respectively. Again, it can be seen that the settings are robust to changing load, and the same setting in both load cases would yield very close to optimal performance.

In order to illustrate the validity of these results, the detailed VSC simulation was carried out with the same settings. Only the capacitor voltage waveforms for nominal load have been presented here due to limited space [see Fig. 7(b)] THDs calculated from the simulation were 2.32 and 2.58%, while f_{sw} were 4.7 and 4.55 kHz. The prediction error of ANN was again less than 3% in all cases.

D. Computational Burden

It is evident that the computational requirements of the proposed method increase exponentially with the increasing number of considered weighting factors. Therefore, there exists practical limit on the number of factors that can be designed in this way. In order to assess this limitation quantitatively, the total duration of stage A was first estimated by extrapolating a duration of a single simulation. To this end, approximately 6 s are necessary to complete 0.06 s of one detailed model simulation on a standard personal computer. In case of two weighting factors, to generate data with high fidelity, 21 values have been chosen for each weighting factor. Therefore, 441 simulations in total were needed to test all the combinations. For carrying out this workload, around 2650 s (44 min) of computational time on a single computer core were needed. However, majority of commercial personal computers have multiple cores and parallelizing the simulation tasks in software like MATLAB is straightforward using the MATLAB/Parallel Computing toolbox. To this end, if the executions were parallelized, 11 min in total were needed on a 4-core processor unit, and only 1.8 min on a 24-core processor. For comparison, if there are three weighting factors in the cost function (assuming again 21 values for each weighting factor), the number of simulations would grow exponentially to 9261. This would make the procedure practically unfeasible to carry out on single core and even on the 4-core processor. However, on the 24-core processor, the overall procedure would be done in less than 40 min. Another possibility to reduce the computational time would be to reduce the fidelity of the weights. For instance, if only ten values for each weighting factor would be used, the data for four weighting factors could be extracted from a 24-core processor in around 40 min. However, it is important to highlight that the number of weighting factors in FS-MPC applications is seldom larger than two, as it can be seen from the list of exemplary cost functions stated in the recent comprehensive review article (e.g., see Table III in [11]). To sum up, it can be concluded that optimization of up to four weighting factors, which covers basically all applications of FS-MPC in power electronics, can be considered as the upper limit with relatively standard hardware.

On the other hand, the number of weighting factors also increases the computational burden of Stage C. However, this increase is not as dramatic as in the case of Stage A, because the evaluation of the feed-forward ANN is computationally very light. For instance, for the case of the ANN with two weighting factors used in this paper, it takes less than 0.125 μ s for one ANN evaluation. This means that super high fidelity fitness function plots (e.g., 4-megapixel plots shown in Figs. 5 and 6 was generated in less than 0.5 s). The optimal solution was then simply obtained by finding the lowest value in the given plot, which can be done in Matlab almost instantaneously using the min function. On the other hand, if the fitness function comprises three or more weighting factors, direct evaluation of ANN with super-high fidelity will become computationally more intensive. For instance, high fidelity evaluation of ANN with three weighting factors (e.g., 500 points for each factor implies $500^3 = 125$ million evaluations) would be done in only 2.5 min. On the other hand, if more weighting factors or more

TABLE III
PERFORMANCE METRICS RESULTS FROM SIMULATIONS, EXPERIMENTS AND ANN PREDICTIONS

	Nominal load				Light load			
	Fitness function	$f_{ann,1}$	$f_{ann,2}$	$f_{ann,1}$	$f_{ann,2}$			
Perf. metrics	THD	f_{sw}	THD	f_{sw}	THD	f_{sw}	THD	f_{sw}
Simulations	1.22%	7.64 kHz	2.32%	4.7 kHz	1.28%	7.7 kHz	2.58%	4.55 kHz
Experiments	1.31%	7.22 kHz	2.31%	5.14 kHz	1.32%	7.6 kHz	2.12%	5.3 kHz
ANN prediction	1.22%	7.71 kHz	2.3%	4.7 kHz	1.21%	7.8 kHz	2.35%	4.99 kHz

fidelity is required to be evaluated, computational time might become impractically long. For this case, there are several alternative ways to do the minimization. First possibility could be to do the fitness function evaluation sequentially. Particularly, the first evaluation could be done with low fidelity to find an area around the optimal point and then using higher and higher fidelity in the following steps to fine tune the solution. In this way, the computational time can be significantly reduced. Another possibility could be to take advantage of the continuous nature of the ANN and perform the gradient descent optimization. This option does not impose almost any limitation on the number of weighting factors, but does entail the risk of getting stuck in the local minimum.

V. EXPERIMENTAL RESULTS

Proposed weighting factor selection strategy was verified experimentally, where the VSC and an *LC* filter structure shown in Fig. 1 was built in the lab. The power stage comprised two Delta Elektronika SM 600-10 dc power supplies connected in series, a Semikron two-level three-phase VSC, an *LC* filter, and a linear load. All the parameters of the setup are listed in Table II. The FS-MPC controller was implemented in the dSpace MicroLabBox with DS1202 PowerPC DualCore 2 GHz processor board and DS1302 I/O board. Delay was remunerated utilizing the strategy given in [31]. Since the overall calculation time was around 15 μ s, the T_s was set to 20 μ s.

A. Validation of Optimal Weighting Factor Design

The experimental results for optimal λ_{der} and λ_{sw} settings for the nominal load [given in Figs. 5(a) and 6(a)] are shown in Fig. 9. The results for optimal λ_{der} and λ_{sw} settings for the light load [given in Figs. 5(b) and 6(b)] are shown in Fig. 10. The obtained results are still considerably well matched with predicted ones by the ANN with less than 10% error in all cases, thus validating the proposed design methodology. The lower precision compared to simulations is attributed to the fact that ANNs were trained using simulation data, where components like semiconductor devices, dc link, and sensors have been modeled ideally. Overall comparison between the results obtained from the detailed simulation model, experimental setup, and the ANN are shown in Table III.

B. Impact of Weighting Factors on Transient Performance

Only steady-state performance metrics has been considered in this paper because the weighting factors turned out to have

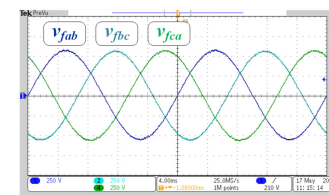
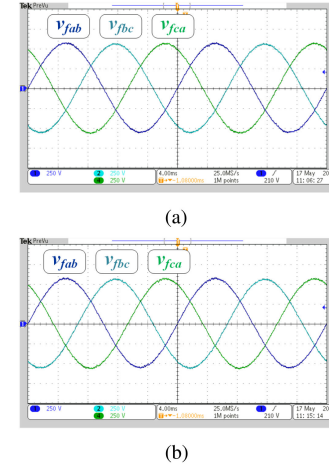


Fig. 9. Experimental line-line capacitor voltage waveforms (v_f : 250 V/div, time axis: 0.4 ms/div) for weighting factors that optimize fitness function (18). (a) Waveforms for nominal load with $\lambda_{der} = 2.005$ and $\lambda_{sw} = 1.605$. Measured THD is 1.31% and f_{sw} is 7.22 kHz. (b) Waveforms for light load with $\lambda_{der} = 2.185$ and $\lambda_{sw} = 2.03$. Measured THD is 1.32% and $f_{sw} = 7.26$ kHz.

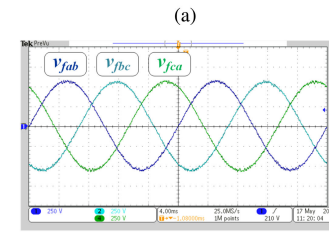
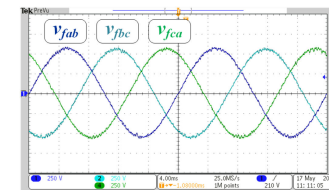


Fig. 10. Experimental line-line capacitor voltage waveforms (v_f : 250 V/div, time axis: 0.4 ms/div) for weighting factors that optimize fitness function (19). (a) Waveforms for nominal load with $\lambda_{der} = 0.8$ and $\lambda_{sw} = 10$. Measured THD is 2.31% and f_{sw} is 5.14 kHz. (b) Waveforms for light load with $\lambda_{der} = 0.85$ and $\lambda_{sw} = 10$. Measured THD is 2.12% and f_{sw} is 5.3 kHz.

a negligible influence on the dynamic performance of the system. In particular, the dominating term during transients in the cost function is the voltage tracking term. On the other hand, the selection of the weighting factors has a significant influence only on the steady-state performance. To verify this, dynamic

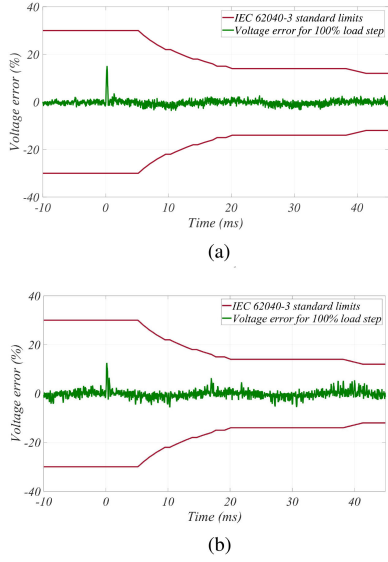


Fig. 11. Experimentally captured transient performance of the output capacitor voltage amplitude error during 100% step change of linear nominal load (according to IEC 62040-3 standard). (a) Voltage error for nominal load with $\lambda_{\text{der}} = 1.605$ and $\lambda_{\text{sw}} = 2.005$. (b) Voltage error for nominal load with $\lambda_{\text{der}} = 0.8$ and $\lambda_{\text{sw}} = 10$.

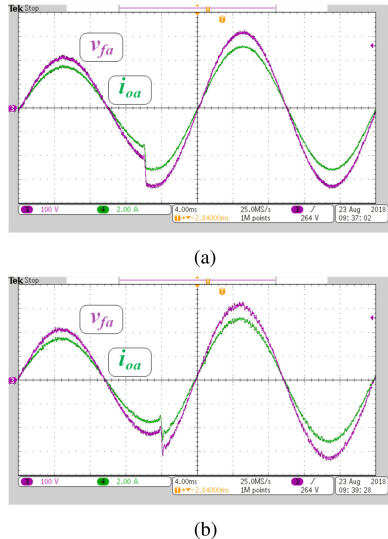


Fig. 12. Experimental output capacitor voltage (v_f : 250 V/div, time axis: 0.4 ms/div) and current (i_o : 2 A/div, time axis: 0.4 ms/div) during the reference step change $v_f^* = 220 \rightarrow 325$ V. (a) Waveforms for nominal load with $\lambda_{\text{der}} = 1.605$ and $\lambda_{\text{sw}} = 2.005$. (b) Waveforms for nominal load with $\lambda_{\text{der}} = 0.8$ and $\lambda_{\text{sw}} = 10$.

performance tests according to the IEC 62040-3 standard for UPS systems have been carried out. Two tests have been done for the 0%–100% step load change (0–6 A) for two weighting factor combinations. As it can be seen from the obtained experimental results (see Figs. 11 and 12), the control method complies with the standard limitations with a large margin, regardless of the weighting factor selection. On the other hand, there exist applications in which the selection of the weighting factors affects the dynamics. One interesting example is [24], where it was shown that increasing the weight associated with

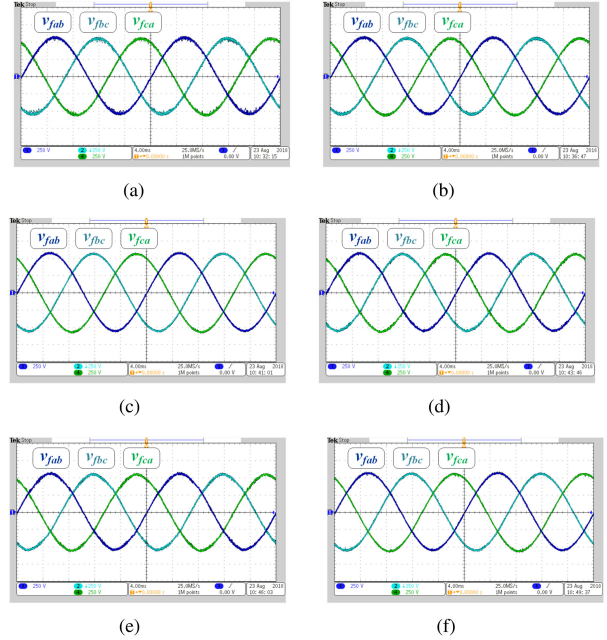


Fig. 13. Experimental line-line capacitor voltage waveforms (v_f : 250 V/div, time axis: 0.4 ms/div) for validation of parameter model uncertainty (nominal values $L_f = 2.4$ mH, $C_f = 15$ μ s) for nominal load with $\lambda_{\text{der}} = 1.605$ and $\lambda_{\text{sw}} = 2.005$. (a) Waveforms for $L_f = 5$ mH, $C_f = 15$ μ s, THD = 2.5%, and $f_{\text{sw}} = 5$ kHz. (b) Waveforms for $L_f = 5$ mH, $C_f = 30$ μ s, THD = 1.92%, and $f_{\text{sw}} = 4.7$ kHz. (c) Waveforms for $L_f = 2.4$ mH, $C_f = 30$ μ s, THD = 1.29%, and $f_{\text{sw}} = 6.7$ kHz. (d) Waveforms for $L_f = 1.2$ mH, $C_f = 15$ μ s, THD = 2.1%, and $f_{\text{sw}} = 8.1$ kHz. (e) Waveforms for $L_f = 1.2$ mH, $C_f = 7.5$ μ s, THD = 2.4% and $f_{\text{sw}} = 9.4$ kHz. (f) Waveforms for $L_f = 2.4$ mH, $C_f = 7.5$ μ s, THD = 1.26%, and $f_{\text{sw}} = 8$ kHz.

one of the weighting factors improves the phase margin of the system. Therefore, phase margin could be also included as a performance metric in that application.

C. Robustness to LC Filter Parameter Variations

Robustness of the optimal weighting factor combinations to internal model parameter variations has also been demonstrated experimentally. Tests have been carried out for the cases of overestimated (two times higher) and underestimated (two times lower) filter parameters (L_f and C_f) for one exemplary set of the optimal weighting factors ($\lambda_{\text{der}} = 1.605$, $\lambda_{\text{sw}} = 2.005$). As it can be seen from the obtained waveforms, the control algorithm is very robust to parameter uncertainties. Algorithm is especially robust if it uses overestimated capacitor values [see Fig. 13(c)]. For overestimated inductance values [see Fig. 13(a)], one can notice a higher ripple in voltage waveforms. The algorithm tracking performance was also not degraded if underestimated capacitor and inductor values were used [see Figs. 13(d) and (e)].

VI. CONCLUSION

In this work, we have presented a novel method for automated selection of the weighting factors in the cost function of the FS-MPC algorithm. The effectiveness of the approach was shown on an exemplary UPS VSC application, although the

methodology is generic and could be applied to any weighting factor based MPC regulated power converter. The method makes use of an ANN to provide a powerful and fast optimization. Further investigation showed that the predicted responses from the network model match very well with the responses derived from the detailed model (less than 3% error) and fairly well with ones derived from the experimental setup (less than 10% error) and that selected weighting factors are robust to load variations. A possible direction for future work could be the design of filters for converters operating at variable switching frequency.

REFERENCES

- [1] F. Blaabjerg, Z. Chen, and S. Kjaer, "Power electronics as efficient interface in dispersed power generation systems," *IEEE Trans. Power Electron.*, vol. 19, no. 5, pp. 1184–1194, Sep. 2004.
- [2] T. Dragicevic, X. Lu, J. C. Vasquez, and J. M. Guerrero, "DC microgrids—Part II: A review of power architectures, applications, and standardization issues," *IEEE Trans. Power Electron.*, vol. 31, no. 5, pp. 3528–3549, May 2016.
- [3] F. Blaabjerg, R. Teodorescu, M. Liserre, and A. V. Timbus, "Overview of control and grid synchronization for distributed power generation systems," *IEEE Trans. Ind. Electron.*, vol. 53, no. 5, pp. 1398–1409, Oct. 2006.
- [4] J. Rodriguez *et al.*, "Predictive current control of a voltage source inverter," *IEEE Trans. Ind. Electron.*, vol. 54, no. 1, pp. 495–503, Feb. 2007.
- [5] P. Cortes, G. Ortiz, J. I. Yuz, J. Rodriguez, S. Vazquez, and L. G. Franquelo, "Model predictive control of an inverter with output lc filter for UPS applications," *IEEE Trans. Ind. Electron.*, vol. 56, no. 6, pp. 1875–1883, Jun. 2009.
- [6] P. Acuna, L. Moran, M. Rivera, J. Dixon, and J. Rodriguez, "Improved active power filter performance for renewable power generation systems," *IEEE Trans. Power Electron.*, vol. 29, no. 2, pp. 687–694, Feb. 2014.
- [7] T. Geyer and D. E. Quevedo, "Performance of multistep finite control set model predictive control for power electronics," *IEEE Trans. Power Electron.*, vol. 30, no. 3, pp. 1633–1644, Mar. 2015.
- [8] B. S. Riar, J. Scoltock, and U. K. Madawala, "Model predictive direct slope control for power converters," *IEEE Trans. Power Electron.*, vol. 32, no. 3, pp. 2278–2289, Mar. 2017.
- [9] S. Bayhan, M. Trabelsi, H. Abu-Rub, and M. Malinowski, "Finite-control-set model-predictive control for a quasi-z-source four-leg inverter under unbalanced load condition," *IEEE Trans. Ind. Electron.*, vol. 64, no. 4, pp. 2560–2569, Apr. 2017.
- [10] T. Dragicevic, "Model predictive control of power converters for robust and fast operation of ac microgrids," *IEEE Trans. Power Electron.*, vol. 33, no. 7, pp. 6304–6317, Jul. 2018.
- [11] S. Vazquez, J. Rodriguez, M. Rivera, L. G. Franquelo, and M. Norambuena, "Model predictive control for power converters and drives: Advances and trends," *IEEE Trans. Ind. Electron.*, vol. 64, no. 2, pp. 935–947, Feb. 2017.
- [12] P. Cortes, J. Rodriguez, D. E. Quevedo, and C. Silva, "Predictive current control strategy with imposed load current spectrum," *IEEE Trans. Power Electron.*, vol. 23, no. 2, pp. 612–618, Mar. 2008.
- [13] M. Aguirre, S. Kouro, C. A. Rojas, J. Rodriguez, and J. I. Leon, "Switching frequency regulation for FCS-MPC based on a period control approach," *IEEE Trans. Ind. Electron.*, vol. 65, no. 7, pp. 5764–5773, Jul. 2018.
- [14] L. Tarisciotti, P. Zanchetta, A. Watson, J. C. Clare, M. Degano, and S. Bifaretti, "Modulated model predictive control for a three-phase active rectifier," *IEEE Trans. Ind. Appl.*, vol. 51, no. 2, pp. 1610–1620, Mar. 2015.
- [15] S. Vazquez, A. Marquez, R. Aguilera, D. Quevedo, J. I. Leon, and L. G. Franquelo, "Predictive optimal switching sequence direct power control for grid-connected power converters," *IEEE Trans. Ind. Electron.*, vol. 62, no. 4, pp. 2010–2020, Apr. 2015.
- [16] R. Vargas, P. Cortes, U. Ammann, J. Rodriguez, and J. Pontt, "Predictive control of a three-phase neutral-point-clamped inverter," *IEEE Trans. Ind. Electron.*, vol. 54, no. 5, pp. 2697–2705, Oct. 2007.
- [17] P. Cortes *et al.*, "Guidelines for weighting factors design in model predictive control of power converters and drives," in *Proc. IEEE Int. Conf. Ind. Technol.*, pp. 1–7.
- [18] P. Zanchetta, "Heuristic multi-objective optimization for cost function weights selection in finite states model predictive control," in *Proc. Workshop Predictive Control Elect. Drives Power Electron.*, Oct. 2011, pp. 70–75.
- [19] S. A. Davari, D. A. Khaburi, and R. Kennel, "An improved FCS-MPC algorithm for an induction motor with an imposed optimized weighting factor," *IEEE Trans. Power Electron.*, vol. 27, no. 3, pp. 1540–1551, Mar. 2012.
- [20] F. Villarroel, J. R. Espinoza, C. A. Rojas, J. Rodriguez, M. Rivera, and D. Sbarbaro, "Multiobjective switching state selector for finite-states model predictive control based on fuzzy decision making in a matrix converter," *IEEE Trans. Ind. Electron.*, vol. 60, no. 2, pp. 589–599, Feb. 2013.
- [21] E. Fuentes, C. A. Silva, and R. M. Kennel, "MPC implementation of a quasi-time-optimal speed control for a PMSM drive, with inner modulated-FS-MPC torque control," *IEEE Trans. Ind. Electron.*, vol. 63, no. 6, pp. 3897–3905, Jun. 2016.
- [22] P. Karamanakos, T. Geyer, and R. Kennel, "A computationally efficient model predictive control strategy for linear systems with integer inputs," *IEEE Trans. Control Syst. Technol.*, vol. 24, no. 4, pp. 1463–1471, Jul. 2016.
- [23] P. Cortes, J. Rodriguez, S. Vazquez, and L. G. Franquelo, "Predictive control of a three-phase UPS inverter using two steps prediction horizon," in *Proc. IEEE Int. Conf. Ind. Technol.*, Mar. 2010, pp. 1283–1288.
- [24] T. Dragicevic, "Dynamic stabilization of dc microgrids with predictive control of point of load converters," *IEEE Trans. Power Electron.*, vol. 33, no. 12, pp. 10872–10884, Dec. 2018.
- [25] J. Schmidhuber, "Deep learning in neural networks: An overview," *Neural Netw.*, vol. 61, pp. 85–117, 2015.
- [26] B. Singh, V. Verma, and J. Solanki, "Neural network-based selective compensation of current quality problems in distribution system," *IEEE Trans. Ind. Electron.*, vol. 54, no. 1, pp. 53–60, Feb. 2007.
- [27] Q.-J. Zhang, K. C. Gupta, and V. K. Devabhaktuni, "Artificial neural networks for RF and microwave design—From theory to practice," *IEEE Trans. Microw. Theory Tech.*, vol. 51, pp. 1339–1350, no. 4, Apr. 2003.
- [28] H. Kabir, Y. Wang, M. Yu, and Q. J. Zhang, "Neural network inverse modeling and applications to microwave filter design," *IEEE Trans. Microw. Theory Tech.*, vol. 56, pp. 867–879, Apr. 2008.
- [29] K. Hornik, M. Stinchcombe, and H. White, "Multilayer feedforward networks are universal approximators," *Neural Netw.*, vol. 2, no. 5, pp. 359–366, 1989.
- [30] D. E. Rumelhart, G. E. Hinton, and R. J. Williams, "Learning representations by back-propagating errors," *Nature*, vol. 323, pp. 533–536, Oct. 1986.
- [31] P. Cortes, J. Rodriguez, C. Silva, and A. Flores, "Delay compensation in model predictive current control of a three-phase inverter," *IEEE Trans. Ind. Electron.*, vol. 59, no. 2, pp. 1323–1325, Feb. 2012.



Tomislav Dragičević (S'09–M'13–SM'17) received the M.Sc. and the industrial Ph.D. degrees in electrical engineering from the Faculty of Electrical Engineering and Computing, University of Zagreb, Zagreb, Croatia, in 2009 and 2013, respectively.

From 2013 to 2016, he was a Postdoctoral Research Associate with Aalborg University, Aalborg, Denmark, where he has been an Associate Professor since March 2016. He was a Guest Professor with Nottingham University, U.K., during spring/summer of 2018. He has authored and coauthored more than 140 technical papers (more than 55 of them are published in international journals, mostly IEEE transactions) in his domain of interest and 8 book chapters and a book in the field. His research interest includes overall system design of autonomous and grid connected dc and ac microgrids, and application of advanced modeling and control concepts to power electronic systems.

Dr. Dragicevic serves as an Associate Editor for the IEEE TRANSACTIONS ON INDUSTRIAL ELECTRONICS and in the *Journal of Power Electronics*. He is a recipient of the Koncar prize for the best industrial Ph.D. dissertation in Croatia, and the Robert Mayer Energy Conservation Award.



Mateja Novak (S'17) received the M.Sc. degree in electrical engineering and information technology from Zagreb University, Zagreb, Croatia, in 2014. She is currently working toward the Ph.D. degree in power electronics with Aalborg University, Aalborg, Denmark.

Her research interests include finite control set model predictive control, multilevel converters, statistical model checking, and renewable energy systems.